High flexibility of DNA on short length scales probed by atomic force microscopy

PAUL A. WIGGINS[1], THIJN VAN DER HEIJDEN[2], FERNANDO MORENO-HERRERO[2], ANDREW SPAKOWITZ[3], ROB PHILLIPS[4], JONATHAN WIDOM[5], CEES DEKKER[2] AND PHILIP C. NELSON[6]*

[1]Whitehead Institute, Cambridge, Massachusetts 02142, USA
[2]Kavli Institute of NanoScience, Delft University of Technology, Lorentzweg 1, 2628 CJ Delft, The Netherlands
[3]Department of Chemical Engineering, Stanford University, Stanford, California 94305, USA
[4]Division of Engineering and Applied Science, California Institute of Technology, Pasadena, California 91125, USA
[5]Department of Biochemistry, Molecular Biology, and Cell Biology, Northwestern University, Evanston, Illinois 60208, USA
[6]Department of Physics and Astronomy, University of Pennsylvania, Philadelphia, Pennsylvania 19104, USA
*e-mail: nelson@physics.upenn.edu

Published online: 3 November 2006; doi:10.1038/nnano.2006.63

The mechanics of DNA bending on intermediate length scales (5–100 nm) plays a key role in many cellular processes, and is also important in the fabrication of artificial DNA structures, but previous experimental studies of DNA mechanics have focused on longer length scales than these. We use high-resolution atomic force microscopy on individual DNA molecules to obtain a direct measurement of the bending energy function appropriate for scales down to 5 nm. Our measurements imply that the elastic energy of highly bent DNA conformations is lower than predicted by classical elasticity models such as the worm-like chain (WLC) model. For example, we found that on short length scales, spontaneous large-angle bends are many times more prevalent than predicted by the WLC model. We test our data and model with an interlocking set of consistency checks. Our analysis also shows how our model is compatible with previous experiments, which have sometimes been viewed as confirming the WLC.

The WLC model of DNA conformation is an effective theory that idealizes the macromolecule as an inextensible elastic rod, and attributes to its bending deformations a classical (Hooke-law-type) elastic energy cost. The WLC has come to dominate physical discussions of double-stranded DNA mechanics, due in part to its simplicity and its successful description of experiments such as force spectroscopy on single DNA molecules[1–3]. Because of these notable successes, classical elasticity models like the WLC (and its generalizations to include twist stiffness) have been the framework for many studies of DNA mechanics. However, previous tests of the WLC model using DNA stretching, atomic force microscopy (AFM) and other methods have been largely insensitive to the details of mechanics in the intermediate-scale regime crucial for cellular function, from chromosomal DNA packaging, to transcription, gene regulation and viral packaging[4–6]. A quantitative understanding of such interactions requires a model of DNA bending that is valid on these biologically relevant length scales.

In the following, we will argue that the successes of the WLC model in fact arise from the long length scales probed by the classic experiments, rather than from any true underlying classical elasticity of DNA, and we will give short-scale measurements that do not agree with the predictions of the WLC model. It may seem that a more general model, capable of embracing both our new data and the classic earlier experiments, would necessarily contain many more unknown parameters than the WLC model. On the contrary, the model we propose is as simple as the WLC.

RESULTS

THE WLC

The WLC model can be formulated more precisely by representing each conformation as a chain of segments of length ℓ and assigning to it an elastic energy cost of the form $E_{WLC} = \frac{1}{2}k_BT(\xi/\ell)(\theta_i)^2$, where θ_i is the angle between successive segment orientations $\mathbf{t}_i$ and $\mathbf{t}_{i+1}$ (in radians), k_BT is the thermal energy, and $\xi \approx 50$ nm is an effective elastic constant describing the chain's resistance to bending (see Supplementary Information). We call this bending-energy function classical (or 'harmonic'), because it is a quadratic function of the strain variable θ_i. The probability distribution of bends is then given by the Boltzmann distribution, $g(\mathbf{t}_{i+1}|\mathbf{t}_i) = q^{-1}\exp[-E_{\mathrm{WLC}}(\theta_i)/k_BT]$, where q is a normalization constant.

The choice of a harmonic energy function E_{WLC} makes the WLC angular distribution gaussian. However, even if $E(\theta)$ is not harmonic, the angular distribution $g(\mathbf{t}_{i+n}|\mathbf{t}_i)$ will approach a gaussian form at large separations $L = n\ell$, because the iterated convolution of any distribution with itself converges to a gaussian form. That is, even if non-harmonic elastic behaviour is present, it will be hidden on long length scales by thermal fluctuations,

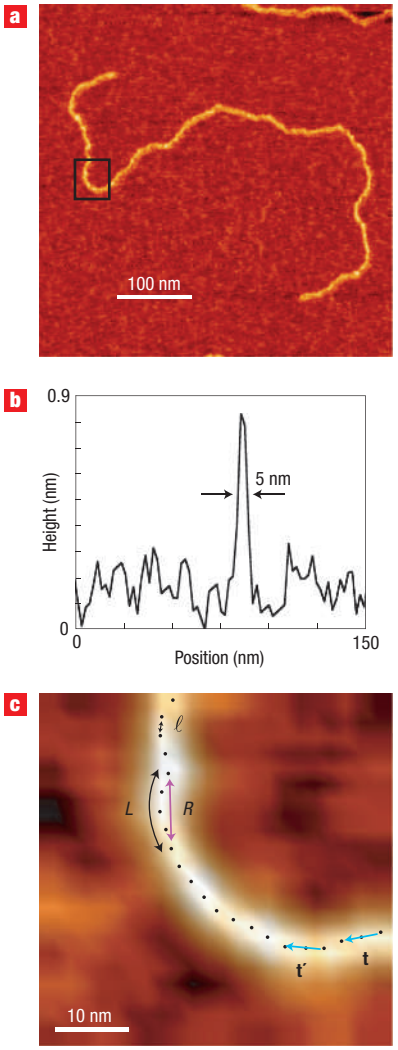

Figure 1 High-resolution AFM images and tracing. Data shown were taken on V4-grade mica with 12 mM Mg^{2+} (see Supplementary Information for other surfaces and salt concentrations). **a**, A 0.5 × 0.5 μm AFM image (256 × 256 pixels) of 2,743-bp dsDNA deposited on mica; *z*-range 1.5 nm. **b**, Cross-sectional height profile of the DNA molecule, showing a half width at half maximum of only 2.5 nm. **c**, Detail of the square section indicated in **a**, showing also the chain of points determined by our automated image-analysis routine and illustrating the geometric quantities discussed in the text. Successive points are separated by $\ell = 2.5$ nm. The end–end distribution $K(R; L)$ is the probability distribution of real-space separation R among points separated by contour length L; in the example in the centre of the figure, we take $L = 4 \times 2.5$ nm. The angle distribution $G(\theta; L)$ is the probability distribution of angles between tangents (short blue arrows) separated by L, which in the example on the right of the figure is 3×2.5 nm.

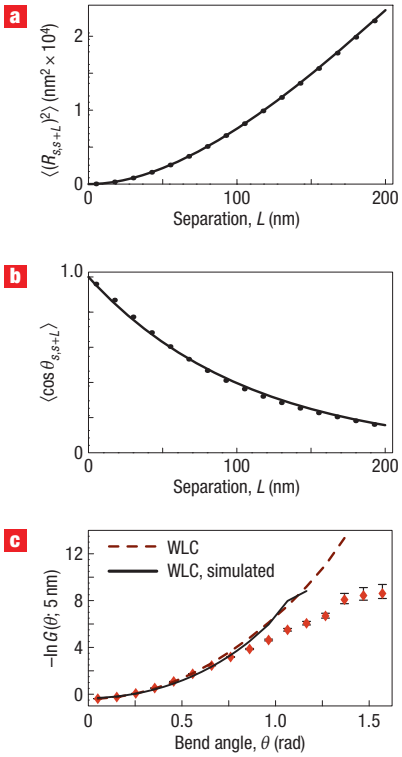

Figure 2 Checks of equilibrium adsorption and failure of WLC on short length scales. a,**b**, Plots of $\langle (R_{s,s+L})^2 \rangle$ and $\langle \cos \theta_{s,s+L} \rangle$ from experimental data (dots), together with model-independent predictions assuming $\xi = 54$ nm (curves). **c**, Dots: negative logarithm of the observed probability distribution function $G(\theta; L = 5\text{ nm})$, a measure of the effective bending energy at this length scale in units of $k_B T$. The graph is a histogram, computed using experimentally observed DNA contours with total length of about 240,000 nm, or a total of about 94,000 pairs of tangent vectors. The error bars represent expected $\sqrt{n}$ error in bin populations due to finite sample size. Dashed curve: the same quantity for curves drawn from the distribution appropriate to the WLC with persistence length equal to that used to draw the curves in (**a** and **b**). Although the two distributions agree qualitatively at low deflection θ, they disagree at large angles: the WLC model predicts far fewer such large deflections than were observed. Solid black curve: the same quantity when a sample of WLC configurations was generated numerically and converted to simulated AFM data, then subjected to the same image analysis that yielded the experimental dots.

giving rise to a theory that behaves like the WLC. Thus, to investigate whether $E(\theta)$ is harmonic, we must measure it directly on the length scale of interest, and not on some much longer scale.

AFM MEASUREMENTS OF DNA CONTOURS

We argued above that to look behind the WLC model, we must examine length scales that are not much longer than the few nanometres scale of the molecule. It is difficult to obtain full three-dimensional views of equilibrium conformations of DNA in solution with the required resolution. However, under appropriate conditions, DNA adheres to a mica surface weakly enough that DNA–mica interactions are believed not to affect the chain statistics[7]. We will argue in the following that our molecules indeed adopt two-dimensional equilibrium conformations. We captured these by using AFM, following procedures outlined in ref. 8, but with significant improvements in image analysis (see 'Methods' and Supplementary Information). Figure 1a is a representative image of DNA on mica, taken using tapping-mode AFM in air. The use of ultrasharp silicon tips allows a very high resolution to be obtained; for example, Fig. 1b displays a cross-sectional DNA height profile with a half width at half maximum of only 2.5 nm.

Despite our many precautions, we realized that potential gradients occur upon DNA adsorption that could potentially

generate spurious results. For this reason, we first made some detailed, model-independent theoretical predictions and checked that they were well obeyed by our data. As a first check, we measured the mean-square separation of pairs of points located at contour length s and $s+L$ from the end of the molecule, averaging over s and over all observed contours. We call this quantity $\langle (R_{s,s+L})^2 \rangle$, and examine its behaviour as a function of the contour length separation L between the points (Fig. 2a). If the chain conformations are indeed equilibrated, and the effective elastic-energy function is local, then this function must take a particular form (see Supplementary Information). Indeed, as Fig. 2a shows, we found that the data follow this prediction very well. We can also define the tangent–tangent correlation $\langle \cos \theta_{s,s+L} \rangle$, where $\theta_{s,s+L}$ is the angle between tangent vectors at a pair of points separated by L. If the chains' conformations are equilibrated, then this correlation must fall with contour separation L as $e^{-L/(2\xi)}$. Figure 2b shows that this prediction, too, is well satisfied, with $\xi = 54$ nm. Together, these two tests confirm that, at least over length scales less than 200 nm, our contours reflect equilibrium two-dimensional chain conformations, extending the observation of Rivetti *et al.*[7].

The statistical measures in Fig. 2a, b are model-independent; they do not distinguish between different forms of the local elastic energy $E(\theta)$. Therefore, we next measured the probability distribution function $G(\theta; 5\,\text{nm})$ of various bend angles at points separated by contour length 5 nm. Figure 2c shows the negative logarithm of this histogram. The resulting curve measures the effective bending energy $E(\theta)/k_BT$, coarse-grained to the length scale $\ell_{exp} = 5$ nm probed by the experiment. As explained above, the WLC model predicts that this function will be quadratic, regardless of the value of ℓ_{exp}. Instead, Fig. 2c shows that the coarse-grained bending energy is far from being a quadratic function of the deflection angle θ. At large angles we see instead that $\ln G(\theta)$ is nearly linear in θ. These results can be stated differently by saying that large angular deflections between points separated by 5 nm were about 30 times more frequent in our data than the prediction of the WLC model (Table 1).

ANHARMONIC MODEL

We constructed a local-elasticity model, with an effective bending-energy function chosen to mimic the behaviour seen in Fig. 2c. This model falls into a large class we have named 'sub-elastic chain' (SEC), because it describes a polymer chain with a response to bending that, for large deflections, is softer than the usual harmonic model[9]. One empirical energy function that summarizes the data is a linear SEC (LSEC):

$$E_{LSEC}(\theta) = \alpha|\theta|k_BT, \qquad (1)$$

where α is a dimensionless constant that depends on the chosen segment length ℓ. We chose $\ell = 2.5$ nm and adjusted α to fit the long-distance correlation $G(\theta; 30\,\text{nm})$, yielding $\alpha = 6.8$. We then reasoned that, if indeed our contours represent equilibrium conformations of an elastic body, and in particular if successive chain elements are independently distributed according to equation (1), then the angle–angle correlations at all separations $L \geq \ell_{exp}$ must be computable from that rule, with no further fitting. Figure 3 tests our predictions for $G(\theta; L)$, and also for the end-to-end distribution $K(R; L)$ defined in Fig. 1c. The remaining five curves in Fig. 3 are zero-fit-parameter predictions of our model and are observed to describe the data very well. The fact that our simple model passes the interlocking set of hurdles represented by the six curves in Fig. 3 is further strong evidence that we indeed measured spontaneous, equilibrium conformational fluctuations characterized by equation (1), and not an instrumental artifact or a surface-adsorption effect. Moreover, in keeping with the expectations raised earlier, these figures show that at large contour-length separations the distribution of bending angles does converge to that expected from the WLC model.

Our model correctly reproduces the existing successes of the WLC model. For example, the force–extension relation in our model is experimentally indistinguishable from that of the WLC model, as is the rate of cyclization for linear constructs longer than a few persistence lengths (see Supplementary Information).

Table 1 Incidence of bends that are large (≥1.1 rad) or medium-large (≥0.8 rad), at contour separations $L = 5$ nm and 10 nm. The first three rows restate points made in the figures. Each of the columns labelled 'fraction' show that our data disagree significantly with the predictions of the WLC model (Fig. 2c), but agree with our model (Fig. 3a). The angles quoted refer to the angle between the vectors t and t′ in Fig. 1c. Row 1: experimental results from our main data. The large absolute numbers emphasize that our conclusions are not merely based on a handful of images. Row 2: expected results from a Monte Carlo evaluation of the WLC model with persistence length $\xi = 54$ nm. Row 3: expected results from Monte Carlo evaluation of our model with the same long-scale behaviour. The remaining rows show results of control experiments and a more detailed calculation (see Supplementary Information). Row 4: experimental data obtained using DNA incubated with ligase. Row 5: experimental data obtained when DNA was adsorbed to V1-grade mica. Row 6: numerical results when the WLC configurations generated by the Monte Carlo code (row 2) were converted to simulated AFM traces and then sent through our image analysis (solid curve in Fig. 2c and Supplementary Information, Fig. S8).

	Points separated by $L = 5$ nm					Points separated by $L = 10$ nm		
	No. of pairs	No. of large bends	Fraction $\times 10^4$	No. of medium bends	Fraction $\times 10^4$	No. of pairs	No. of large bends	Fraction $\times 10^4$
Experimental data	93,895	82	8.7	746	79	92,725	969	100
WLC	3,122,109	91	0.29	6,848	22	3,105,187	17,678	57
LSEC equation (1)	2,922,111	2,756	9.4	21,809	75	2,906,273	28,773	99
Experimental with ligase	51,303	42	8.2	469	91	50,699	467	92
Experimental with V1-grade mica	30,597	18	5.9	263	86	30,263	326	110
WLC simulated	200,152	11	0.55	568	28	185,164	1,089	59

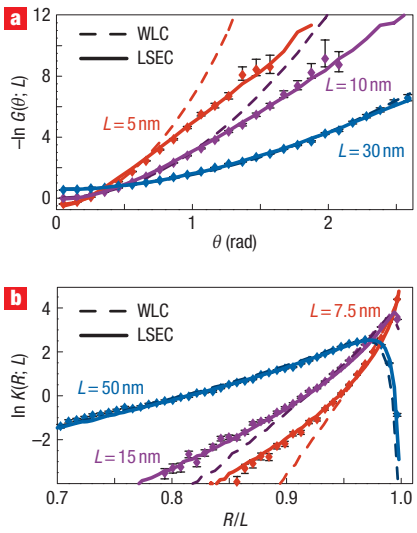

Figure 3 The non-harmonic elasticity model of equation (1) simultaneously fits many statistical properties of the experimental data. a, Negative logarithm of the probability distribution function $G(\theta; L)$ for the angle θ between tangents separated by contour length L, for $L = 5$ nm (orange), 10 nm (purple) and 30 nm (blue). The dots are experimental data; the red dots, and the meaning of the error bars, are the same as in Fig. 2c. Solid curves: Monte Carlo evaluation of this correlation function in our model (equation (1)). Dashed curves: Monte Carlo evaluation of the same correlation in the WLC model with persistence length $\xi = 54$ nm. The dashed curves are all parabolas. The red dashed line is the same as in Fig. 2c. Although the WLC model can reproduce the observed correlation at long separations, at short and medium separation it understates the prevalence of large-angle bends. **b**, Logarithm of the probability distribution function $K(R; L)$, expressed in nm^{-1}, for the real-space distance R between points separated by contour length $L = 7.5$ nm (orange), 15 nm (purple) and 50 nm (blue). As in **a**, the WLC model correctly captures the long-distance behaviour, but understates large bending (leading to large shortening) at separations less than about half a persistence length.

DISCUSSION

Other authors have already reported that AFM images confirm that adsorbed DNA follows a two-dimensional WLC distribution[7]. Indeed we agree, when DNA is viewed on long length scales. However, we find significant deviations from the WLC model on shorter, biologically relevant, length scales. It is possible in principle that surface adsorption and local defects on mica could conspire to modify the apparent elasticity of DNA. Our many checks and controls make this unlikely, however (for example, those shown in Fig. 2a, b). Other experiments not involving AFM, as well as molecular simulations, also point to a modification of the WLC model qualitatively similar to the one we report here (see Supplementary Information).

Our empirical effective bending-energy function, embodied in equation (1), is as simple as the WLC model, and yet unlike the WLC model it accurately describes the observed behaviour of DNA on multiple length scales, at both high and low curvatures. In particular, it is a useful starting point for the description of regulatory loops and other mesoscale DNA complexes. Our generic viewpoint, using models of the SEC type, may also be applicable to other stiff biopolymers.

The form of the effective coarse-grained energy function that we find (equation (1)) may come as a surprise, but in fact there is a precedence for functions of this form. For example, the overstretching transition of DNA reveals a plateau in the force–extension relation, created by a transition between effective links of two different types, with different values of the rise per base pair[10]. Another transition leads to a nearly constant axial torque as DNA under tension is twisted[11]. Although these dramatic transitions occur in the laboratory at high external stresses, they will also occur spontaneously, albeit infrequently, and may in fact mediate important functions of DNA[12,13]. By analogy, we can imagine a transition between two or more conformers with different bend angle (or stiffness), for example, the bent, but still base-paired, state constructed long ago by Crick and Klug[14]. Increasing the bending stress on a tract of the molecule could then alter the coexistence between the conformers, leading to a plateau in the stress–strain relation, or in other words an effectively linear energy function for bend. There may be a threshold for the onset of this approximately linear behaviour; the effective elastic energy function may have a harmonic (parabolic) region at small curvature. However, we found that the harmonic-elasticity regime, if any, is small (see Supplementary Information). In any case, the presence of such a regime is not needed to account for previously known facts about DNA mechanics (see Supplementary Information).

An alternative possibility is that 'bare' DNA elasticity may in fact be harmonic, but it is dressed into a non-harmonic form by electrostatic effects, which have already saturated at the lowest Mg^{2+} concentrations we studied. For example, Rouzina and Bloomfield proposed that the presence of multivalent cations in solution could lead to transient kinking of DNA[15]. Because their effect is non-local only over about six base pairs, it would appear local when coarse grained to length scales longer than about 2 nm, and so can be described using the methods of this paper. Indeed, one benefit of our coarse-grained approach is that our empirical effective energy function is useful even before we resolve its mechanistic origin.

One key application of this work is in biological systems, where DNA–protein complexes are important for the molecular-scale function of the cell. Many authors have assumed that for small loops, where thermal fluctuations may be neglected, classical harmonic rod elasticity is still applicable. On the contrary, we suggest that the WLC model, when it is useful, actually owes its applicability to the existence of thermal fluctuations; when fluctuations can be neglected, then we must use a non-harmonic energy function like equation (1).

In summary, we have argued that the short-length-scale bend distribution function must be measured directly, not extrapolated from long-length-scale measurements. We made such measurements, and showed that the probability of spontaneous sharp bending is orders of magnitude higher than predicted by the WLC model. However, we found that a surprisingly simple coarse-grained elasticity theory is quantitatively accurate, both for describing spontaneous conformational fluctuations of DNA on length scales relevant for looping and nucleosome formation (5 nm and longer), and for the force–extension of DNA and other long-length-scale phenomena.

METHODS

SAMPLE PREPARATION AND AFM

DNA samples were prepared for AFM imaging by depositing 5 ng 2,743-bp linear double-stranded DNA (pGEM-3Z, Promega) diluted in 6 μl of 10 mM Tris–HCl (pH 8.0), supplemented with either 6, 12, 30 or 150 mM $MgCl_2$, onto freshly cleaved muscovite-form mica of grade V1 and V4 (SPI), following the methods of other authors[7,8,16]. After approximately 30 s, the mica was washed with MilliQ-filtered water and blown dry in a gentle stream of nitrogen gas. Samples were imaged in air at room temperature and humidity with a NanoScope IIIa (Digital Instruments), operating in tapping mode with a

type-E scanner, with a pixel size (grid spacing) of 1.95 nm. Background correction consisted of fitting a second-order polynomial to every line in the AFM image. Tapping-mode SuperSharpSilicon tips, type SSS-NCH-8 (NanoSensors) were used. Some of the experiments were carried out using a commercial AFM from Nanotec Electronica operating in dynamic mode (see Supplementary Information). For both the Digital Instruments set-up and the configuration from Nanotec Electronica we obtained similar results, thus excluding artifacts caused by the imaging instrument.

The surface and DNA were free of any salt deposits or protein impurities, and very clean images of DNA were obtained. Furthermore, we studied the effect of repairing possible nicks using ligase, examined various qualities of mica, and systematically varied the concentration of Mg^{2+} in the solution. None of these variations altered our conclusions (see Supplementary Information and Table 1). We note that Mg^{2+} concentrations at the lower end of the range we checked have been found to reduce the persistence length of DNA only slightly[17,18].

IMAGE ANALYSIS

Our image-analysis software was custom developed with the particular goal of analysing the local bend angles. The DNA molecules were traced automatically (but with human supervision) using a custom code in Matlab. Chain tracing was initiated at a user-determined initial point and trial tangent direction. (See Supplementary Information for a description of the algorithm.) Its output was a representation of the DNA contours as chains of *xy* pairs separated by contour length 2.5 nm (Fig. 1c).

DATA ANALYSIS

To reduce the effects of noise, we looked at the real-space separations of points separated by at least three steps (7.5 nm; see Fig. 3b), and the angular difference between tangent vectors defined by next-nearest neighbours and separated by at least two steps (5 nm; see Figs. 1c and 3a). We also applied the same procedures to virtual chains generated by our Monte Carlo code (see Supplementary Information), and made appropriate comparisons.

We performed extensive tests to support our interpretation of the data. We checked by eye that our contour-tracking software faithfully followed the contours, and we sent simulated WLC data, including noise and tip-induced broadening, through our image-processing and analysis software to confirm that the resulting WLC-based contours did not generate distributions resembling our experimental data (see Fig. 2c and Supplementary Information). Moreover, we checked that the alternative hypothesis of non-equilibrium adsorption of a WLC-distributed chain to the surface does not explain our experimental data (see Supplementary Information).

Received 23 June 2006; accepted 31 August 2006; published 3 November 2006.

References

1. Bustamante, C., Marko, J. F., Siggia, E. D. & Smith, S. Entropic elasticity of lambda phage DNA. *Science* **265,** 1599–1600 (1994).
2. Bustamante, C., Smith, S. B., Liphardt, J. & Smith, D. Single-molecule studies of DNA mechanics. *Curr. Opin. Struct. Biol.* **10,** 279–285 (2000).
3. Nelson, P. *Biological Physics: Energy, Information, Life* (W. H. Freeman, New York, 2004).
4. Widom, J. Role of DNA sequence in nucleosome stability and dynamics. *Q. Rev. Biophys.* **34,** 269–324 (2001).
5. Rippe, K., von Hippel, P. R. & Langowski, J. Action at a distance: DNA-looping and initiation of transcription. *Trends Biochem. Sci.* **20,** 500–506 (1995).
6. Shore, D., Langowski, J. & Baldwin, R. L. DNA flexibility studied by covalent closure of short fragments into circles. *Proc. Natl Acad. Sci. USA* **170,** 4833–4837 (1981).
7. Rivetti, C., Guthold, M. & Bustamante, C. Scanning force microscopy of DNA deposited onto mica: Equilibration versus kinetic trapping studied by statistical polymer chain analysis. *J. Mol. Biol.* **264,** 919–932 (1996).
8. van Noort, J. *et al.* The coiled-coil of the human rad50 DNA repair protein contains specific segments of increased flexibility. *Proc. Natl Acad. Sci. USA* **100,** 7581–7586 (2003).
9. Wiggins, P. A. & Nelson, P. C. Generalized theory of semiflexible polymers. *Phys. Rev. E* **73,** 031906 (2006).
10. Storm, C. & Nelson, P. Theory of high-force DNA stretching and overstretching. *Phys. Rev. E* **67,** 051906 (2003). Erratum *Phys. Rev E.* **70,** 013902 (2004).
11. Bryant, Z. *et al.* Structural transitions and elasticity from torque measurements on DNA. *Nature* **424,** 338–341 (2003).
12. Leger, J. F., Robert, J., Bourdieu, L., Chatenay, D. & Marko, J. F. RecA binding to a single double-stranded DNA molecule: A possible role of DNA conformational fluctuations. *Proc. Natl Acad. Sci. USA* **95,** 12295–12299 (1998).
13. Sobell, H. M., Tsai, C., Jain, S. C. & Gilbert, S. G. Visualization of drug–nucleic acid interactions at atomic resolution. 3. Unifying structural concepts in understanding drug–DNA interactions and their broader implications in understanding protein–DNA interactions. *J. Mol. Biol.* **114,** 333–365 (1977).
14. Crick, F. H. C. & Klug, A. Kinky helix. *Nature* **255,** 530–533 (1975).
15. Rouzina, I. & Bloomfield, V. A. DNA bending by small, mobile multivalent cations. *Biophys. J.* **74,** 3152–3164 (1998).
16. Hansma, H., Revenko, I., Kim, K. & Laney, D. Atomic force microscopy of long and short double-stranded, single-stranded and triple-stranded nucleic acids. *Nucleic Acids Res.* **24,** 713–720 (1996).
17. Wang, M. D., Yin, H., Landick, R., Gelles, J. & Block, S. M. Stretching DNA with optical tweezers. *Biophys. J.* **72,** 1335–1346 (1997).
18. van der Heijden, T. *et al.* Torque-limited RecA polymerization on dsDNA. *Nucleic Acids Res.* **33,** 2099–2105 (2005).

Acknowledgements

We thank N. R. Dan, N. H. Dekker, M. Inamdar, R. James, R. D. Kamien, I. Kulic, T. Laurence, R. Lavery, J. Maddocks J. Marko, A. Onufriev, P. Purohit, I. Rouzina, J. M. Schurr, R. Seidel, V. Soghomonian, Z.-G. Wang and Y. Zhang for helpful discussions and correspondence. P.A.W. acknowledges grant support from an NSF graduate fellowship. F.M.-H. acknowledges support from La Fundacien Ramon Areces as a postdoctoral fellow. A.J.S. acknowledges funding from the National Institutes of Health (NIH-GM071552). R.P. and P.A.W. acknowledge the Keck Foundation and NSF Grant CMS-0301657 as well as the NSF-funded Center for Integrative Multiscale Modeling and Simulation. J.W. acknowledges support from NIH grants R01 GM054692 and R01 GM058617. C.D. acknowledges the Stichting voor Fundamenteel Onderzoek der Materie (FOM), which is financially supported by the Nederlandse Organisatie voor Wetenschappelijk Onderzoek (NWO). P.N. acknowledges NSF Grant DMR04-04674 and the NSF-funded NSEC on Molecular Function at the Nano/Bio Interface DMR04-25780. J.W., R.P. and P.C.N. acknowledge the hospitality of the Kavli Institute for Theoretical Physics, supported in part by the National Science Foundation under Grant PHY99-07949.

Correspondence and requests for materials should be addressed to P.C.N.

Supplementary information accompanies this paper on www.nature.com/naturenanotechnology.

Author contributions

P.A.W., T.v.d.H., F.M.-H., C.D. and P.N. contributed to the experimental, theoretical and analysis strategy. T.v.d.H. and F.M.-H. carried out the AFM experiments, and with, C.D. and P.A.W. contributed to the custom image-processing software. P.A.W., T.v.d.H., F.M.-H., C.D. and P.C.N. contributed to the analysis. A.S. contributed the analysis and simulations of nonequilibrium adsorption. P.A.W., R.P., J.W. and P.C.N. contributed to the initial formulation of the hypothesis and its refinement. P.W., T.v.d.H., F.M.-H., A.S., C.D. and P.C.N. contributed to the written and graphical presentation; all authors discussed the results and commented on the manuscript.

Competing financial interests

The authors declare that they have no competing financial interests.